Inner-shell 2*p* photoionization and Auger decay of atomic silicon

K. Jänkälä,[1,*] S. Urpelainen,[1,2] M. Huttula,[1] S. Fritzsche,[1,3,4] S. Heinäsmäki,[1] S. Aksela,[1] and H. Aksela[1]
[1]*Department of Physical Sciences, P.O. Box 3000, 90014 University of Oulu, Oulu, Finland*
[2]*Max-lab, Lund University, Box 118, SE-22100 Lund, Sweden*
[3]*Max-Planck-Institut für Kernphysik, D-69029 Heidelberg, Germany*
[4]*Gesellschaft für Schwerionenforschung (GSI), D-64291 Darmstadt, Germany*
(Received 20 March 2008; published 4 June 2008)

A detailed experiment on 2*p* photoionization and subsequent Auger decay of atomic silicon is presented. Fine-structure-resolved photoelectron and Auger electron spectra are interpreted with the aid of large-scale multiconfiguration calculations. Energy separation and the relative cross sections of the 2*p* ionized fine-structure states of Si^+ are given. The complete 2*p* Auger electron spectrum of Si is interpreted, and the intensity distribution to individual doubly ionized final states is studied.

DOI: 10.1103/PhysRevA.77.062504 PACS number(s): 32.10.−f, 32.80.Fb, 32.80.Hd, 31.15.A−

I. INTRODUCTION

The importance of Si in applied physics, semiconductors, and astronomy is hard to overemphasize. Si as a component in metallic clusters [1] and applications to the manipulation of single atoms in surfaces (see, e.g., Ref. [2]) makes information from single Si atoms even more valuable. In order to determine the chemical shifts and modifications to inner-shell photoionization energies and cross sections in molecules and surfaces, the atomic case has to be known as reference. Numerous articles from the 2*p* photoionization of Si in SiX_n compounds, powders, and solids exist (see, e.g., Refs. [3–6] and references therein), but studies of atomic Si are few. The main reason why the 2*p* spectra of Si have not yet been studied is the very high evaporation temperature of approximately 1500 °C needed for providing a vapor pressure on the order of 10^{-3} mbar [7] in the crucible.

So far, the demand for such a high temperature has limited inner-shell studies in Si to the laser-produced plasma technique. The advantage (and disadvantage) of this technique is that the sputtering laser produces merely ions. From these experiments the 2*p* absorption and ionization cross sections of Si^+ and Si^{2+} have been studied in, e.g., Refs. [8–11]. In neutral Si, the works are limited to an experiment by Costello *et al.* [8] who determined indirectly the binding energies of some $2p^{-1}$ fine-structure components from the $2p^6 3s 3p^2 \rightarrow 2p^5 3s^2 3p^2$ absorption spectrum. From this study, the 2*p* ionization threshold of 107.98 eV was determined. This value deviates from earlier studies by van Brug *et al.* [9] (115 ± 4 eV) and Ohyanagi *et al.* [10] (109 ± 1 eV). The lack of experimental information has also limited the theoretical activities in this field, and as far as we know, no calculations besides ionization threshold estimates [10,12] for the 2*p* ionization and subsequent Auger decay of atomic Si exist. In this article we present a comprehensive experimental and theoretical study of 2*p* photoionization and Auger decay of initially neutral atomic Si.

II. EXPERIMENT

The experimental work was carried out at the 1.5-GeV MAX-II synchrotron storage ring at the high-resolution undulator beamline I411 in MAX-laboratory (Lund, Sweden). The electron spectra were measured using a modified Scienta SES-100 electron energy analyzer mounted on the setup built in Oulu [13]. In order to obtain angle-independent intensities, the electron spectra were measured at an angle of 54.7° with respect to the polarization vector of the linearly polarized synchrotron radiation. The beam of Si vapor was produced by using an inductively heated oven system (for a detailed description, see Ref. [14]) at a temperature of 1500 °C. The Si sample was placed into a single-hole tungsten crucible with an opening angle of 30°.

The photoelectron spectra were measured at the photon energy of 140 eV, with a spectrometer constant pass energy of 10 eV. The beamline slit was 30 μm and the spectrometer entrance slit 0.8 mm (curved). With these settings the experimental broadening was about 55 meV. In the two-step approximation, the Auger electron lines are not expected to be sensitive to the photon energy bandwidth well above the ionization threshold. This allowed us to measure the 2*p* Auger spectrum using the first-harmonic undulator peak without monochromatization. The nominal energy of the peak was set to 135 eV. Providing up to two orders of magnitude higher photon flux than with monochromatization, the method has proven to be very efficient also in our previous experiments [15,16]. The high photon flux allowed us to measure the Auger electron spectrum with a 5-eV pass energy. In addition, the 2*p* Auger spectrum was measured also below the first shakeup satellites at the (monochromatized) photon energy of 111 eV. The binding and kinetic energy calibrations were made by using the Xe 4*d* photoelectron lines [17] and $N_{4,5}O_{2,3}O_{2,3}$ Auger electron lines, respectively. The analyzer transmission function was determined experimentally using the constant ratio between the Xe 4*d* photoelectron and Auger electron lines as described in Ref. [18].

III. THEORY AND CALCULATIONS

The calculations were carried out using multiconfiguration Dirac-Fock (MCDF) method by applying the GRASP92 code [19] together with RELCI extension [20]. In the MCDF method, the atomic state functions (ASFs) are represented as linear combinations of *jj*-coupled configuration state func-

*kari.jankala@oulu.fi

tions (CSFs) with the same total angular momentum J_α and parity P_α:

$$|\Psi_\alpha(P_\alpha J_\alpha)\rangle = \sum_k c_{\alpha k} |\psi_k(P_\alpha J_\alpha)\rangle. \quad (1)$$

The coefficients $c_{\alpha k}$ are obtained by diagonalizing the electron-electron interaction matrix which allows the electronic correlations to be taken into account. The wave functions are obtained self-consistently using the Dirac-Coulomb Hamiltonian (for further details, see Ref. [19] and references therein). Because of good *LSJ*-coupling conditions in Si, the inherently *jj*-coupled ASFs were interpreted in the *LSJ* basis. The unitary transform between the two bases was done by applying the program LSJ [21].

The photoionization and Auger amplitudes were determined by utilizing the PHOTO and AUGER components of the RATIP package [22]. The PHOTO component calculates the photoionization amplitudes in the dipole approximation by decomposing the atom-photon interaction matrix into one-electron amplitudes for each pair of CSFs within the given basis. The photoionization cross section is then obtained by summation of amplitudes over all final-state CSFs and the outgoing electron in the continuum. For further details about the PHOTO component the reader is referred to Refs. [15,23]. The Auger decay intensity is given by

$$n_{f\beta} = \frac{2\pi \sum_{l_A j_A} |\sum_{\mu\nu} c_{f\mu} c_{\beta\nu} M^{\mu\nu}_{f\beta}(J_f, J_\beta)|^2}{P_\beta(J_\beta)} Q_\beta(J_\beta), \quad (2)$$

where $M^{\mu\nu}_{f\beta}(J_f, J_\beta)$ is the Coulomb matrix element $\langle \psi_\mu(J_f) \epsilon_A l_A j_A; J_\beta \| \Sigma^{N-1}_{mn} (1/r_{mn}) \| \psi_\nu(J_\beta) \rangle$, $P_\beta(J_\beta)$ is the total decay rate, and $Q_\beta(J_\beta)$ is the $|\Psi(J_i)\rangle \rightarrow |\Psi(J_\beta)\rangle$ ionization cross section. For more details about the AUGER program, see Refs. [22,24,25] and references therein.

At the temperature of 1500 °C three thermally excited states are present in the Si vapor—namely, $[\mathrm{Ne}]3s^2 3p^2\ {}^3P_{0,1,2}$ triplet states. Proportions were calculated from the Boltzmann distribution, giving 12.6% ${}^3P_0$, 35.4% ${}^3P_1$, and 51.8% ${}^3P_2$. Contributions from the higher excited states of the same configuration are 0.05% ${}^1D_2$ and $(3 \times 10^{-7})\%$ ${}^1S_0$.

The calculations were performed by starting from the single-configuration approximation and extending the configuration space stepwise to the limit where reasonable agreement with the experiment was obtained. The final CSF expansion for $2p$-ionized states of Si included odd-parity configurations constructed from $3s^2 3pnl$ and $3s3p^2 nl$ single excitations and $3s^2 nl^2$ and $3p^2 nl^2$ double excitations, where nl goes from $3p$ to $5p$ (excluding $4f$). The total amount of CSFs was then reduced by allowing only CSFs which couple directly to the $2p^5 3s^2 3p^2$ configuration via the Dirac-Coulomb Hamiltonian. The doubly ionized final states included all even- and odd-parity configurations of the type $2p^6 3snl$, $2p^6 3pnl$, and $2p^6 nl^2$ where nl runs from $3s$ to $5p$ (excluding $4f$). The initial states and $2p$ single-ionized states of Si were calculated in an optimal level (OL) scheme by optimizing the configuration energy to the lowest 5 and lowest 21 states, respectively. The Si^{2+} final states were calculated in average level (AL) scheme. In addition, some calculations were repeated in multiconfiguration Hartree-Fock approximation using Cowan's code [26].

TABLE I. Experimental [27] and calculated splitting of the $[\mathrm{Ne}]3s^2 3p^2$ ground-state configuration of atomic Si. Column $|c_1^{LS}|^2$ gives the purities of the leading configurations in *LSJ* coupling.

Experiment [27]		Theory	
Term	ΔE (eV)	ΔE (eV)	$\lvert c_1^{LS}\rvert^2$
${}^3P_0$	0.0	0.0	0.99
${}^3P_1$	0.0096	0.0096	1.00
${}^3P_2$	0.0277	0.0281	0.99
${}^1D_2$	0.7810	1.0273	0.99
${}^1S_0$	1.9087	1.8598	0.99

IV. RESULTS AND DISCUSSION

We start the discussion from the ground-state configuration. Experimental values from Ref. [27] and calculated level splittings of the $[\mathrm{Ne}]3s^2 3p^2$ configuration are listed in Table I, showing also calculated purities in *LSJ* coupling. Nearly pure *LS* coupling results from identically zero Slater exchange interaction integrals for np^2-type configurations [26]. The spin-orbit interaction is, as expected, small for the valence electrons, causing a 27.7-meV splitting in the ${}^3P$ triplet. A maximum of 1.9 eV splitting in the ground-state configuration rises then entirely from the direct Coulomb interaction.

A. 2*p* photoionization of atomic Si

When the $2p$ shell is ionized an additional $2p^{-1}$-$3p^2$ coupling takes place and also a Coulomb exchange interaction becomes possible. The 21 states obtained from coupling of the $2p^{-1}3s^2 3p^2$ configuration are given in Table II, which lists also the experimental intensity-weighted binding energies, level splittings, and relative photoionization intensities at the temperature of 1500 °C. The values were obtained by a two-line least-squares fitting corresponding to ${}^3P_{0,1}$-${}^3P_2$ initial-state splitting. Columns 6–8 show the results from the MCDF calculations for energy-level splittings, relative intensities, and purities in *LSJ* basis. The line numbers refer to the resolved peaks in the experiment shown in Fig. 1(a). According to Figs. 1(a) and 1(b) the main energy-level structure populated in $2p$ photoionization is well described by 21 levels from the single configuration $2p^{-1}3s^2 3p^2$ in *LSJ* coupling and no additional lines arise from the admixture of other configurations. The single-electron dipole operator does not change the initial *LS* coupling of the two $3p$ electrons. Therefore the intensity corresponding a $2p$ hole state with the largest CSF component with parent coupling of ${}^1D$ or ${}^1S$ comes from the basis state mixing with CSFs having a ${}^3P$-coupled parent term. The $2p^6 3s^2 3p^2 \rightarrow 2p^{-1}3s^2 3p4p$ shakeup satellite structure is depicted on the upper left corner of Fig. 1(a). The center of gravity of the satellite structure is located at 121.8 eV binding energy, and the total intensity

TABLE II. Experimental and theoretical energies and relative intensities of the main photoelectron peaks of Si at a temperature of 1500 °C. Assignment denotes the leading $2p^{-1}3s^23p^2$ final-state fine-structure components in *LSJ* notation. Terms in parentheses denote parent *LS* coupling of the $3p^2$ electrons. Final-state numbering refers to peaks in Fig. 1. The intensities are given as percentages from the total area. Column $|c_1^{LS}|^2$ gives the purities of the leading configurations in *LSJ* coupling.

		Experiment			Theory		
Peak	Final state	E_b (eV)	ΔE_b (eV)	Int.	ΔE_b (eV)	Int.	$\lvert c_1^{LS}\rvert^2$
1	$(^3P)\ ^4P_{5/2}$	107.99(4)	0.00	10.64 ± 0.4	0.00	11.41	0.89
2	$(^3P)\ ^4P_{3/2}$	108.11(4)	0.12	7.39 ± 0.3	0.11	8.49	0.84
3	$(^3P)\ ^4P_{1/2}$	108.21(4)	0.23	3.87 ± 0.3	0.23	3.39	0.85
4	$(^3P)\ ^4D_{7/2}$	108.54(4)	0.55	15.27 ± 0.4	0.51	11.95	0.93
5	$(^3P)\ ^4D_{5/2}$	108.67(4)	0.69	15.15 ± 0.6	0.64	14.04	0.74
6	$(^1D)\ ^2P_{1/2}$	108.81(4)	0.83	7.79 ± 0.5	0.74	1.76	0.36[a]
	$(^3P)\ ^4D_{3/2}$				0.75	8.09	0.58
7	$(^1D)\ ^2P_{3/2}$	-	-	-	0.90	3.11	0.35[b]
8	$(^3P)\ ^4D_{1/2}$	109.07(4)	1.08	3.99 ± 0.1	1.07	4.11	0.69
9	$(^3P)\ ^2D_{3/2}$	109.28(4)	1.29	7.51 ± 0.2	1.27	10.56	0.52
10	$(^3P)\ ^2D_{5/2}$	109.42(4)	1.43	10.30 ± 0.3	1.43	8.99	0.74
11	$(^3P)\ ^2S_{1/2}$	109.57(4)	1.58	10.84 ± 0.4	1.57	3.21	0.87
	$(^3P)\ ^4S_{3/2}$				1.60	5.17	0.82
12	$(^1D)\ ^2F_{7/2}$	109.69(5)	1.70	0.22 ± 0.1	1.84	0.004	0.93
13	$(^1D)\ ^2F_{5/2}$	109.85(5)	1.86	0.36 ± 0.1	2.18	0.07	0.70
14	$(^1D)\ ^2D_{5/2}$	110.45(4)	2.46	0.44 ± 0.1	2.80	0.12	0.68
	$(^1D)\ ^2D_{3/2}$				2.83	0.18	0.87
15	$(^1S)\ ^2P_{3/2}$	111.63(6)	3.36	1.14 ± 0.1	3.76	0.03	0.75[c]
16	$(^3P)\ ^2P_{1/2}$	111.69(6)	3.70	0.34 ± 0.1	3.92	0.82	0.35[d]
17	$(^3P)\ ^2P_{1/2}$	112.02(6)	4.04	2.73 ± 0.2	4.33	1.12	0.50[e]
18	$(^1S)\ ^2P_{3/2}$	112.14(6)	4.17	1.93 ± 0.2	4.49	3.38	0.44[f]

[a]State has $(^3P)\ ^2P_{1/2}$ component of $|c_2^{LS}|^2=0.33$.
[b]State has $(^3P)\ ^3P_{3/2}$ component of $|c_2^{LS}|^2=0.34$.
[c]State has $(^1D)\ ^2P_{3/2}$ component of $|c_2^{LS}|^2=0.11$.
[d]State has $(^1D)\ ^2P_{1/2}$ component of $|c_2^{LS}|^2=0.32$.
[e]State has $(^3P)\ ^2P_{1/2}$ component of $|c_2^{LS}|^2=0.26$.
[f]State has $(^1D)\ ^2P_{3/2}$ component of $|c_2^{LS}|^2=0.35$.

ratio between the satellite and the main lines is 0.151. This agrees well with theoretical value of 0.155 obtained using simple sudden approximation method (see, e.g., Ref. [28] and references therein). Detailed analysis of the structure is hampered by the small separation of the different fine-structure components, and further analysis is left for the future work.

Photoionization dipole amplitudes from the lowest initial state to $(^3P)\ ^4P_{5/2}$ state are identically zero, because the $^3P_0$ parent does not couple with the $2p$ hole to form a $J=5/2$ state. Therefore the experimentally observed center of gravity of the corresponding photoline is shifted slightly toward smaller binding energy. We can approximate that the (dipole-forbidden) binding energy for the $2p$ shell from the ground state is about 108.00(4) eV, which is in agreement with 107.98 eV from Ref. [8]. On the other hand, the first observable $2p$ ionization threshold from the ground state is obviously at about 110 meV higher binding energy. The best calculated binding energy of 107.14 eV using GRASP92 was obtained from an OL calculation by optimizing the total energies of the atomic and Si^+ ionic cases to the ground state and the lowest $2p$-ionized state, respectively. In comparison, the binding energy of 107.93 eV using Cowan's code and scaling the Slater integrals to 85% from the *ab initio* values is in nice agreement with the experiment.

Table II and Figs. 1(a) and 1(b) show that the binding energy splitting of peaks 1–12 is predicted exceptionally well. Agreement is worse, however, for the ^2P_J and ^2D_J states at higher binding energy (peaks 14–18). This deviation, often encountered in *ab initio* calculations, is due to an overestimation of the exchange interaction. Spin-orbit splitting between lines with the same L and S lines is well accounted for, except that the splitting of $^2F_{7/2}$ and $^2F_{5/2}$ states is overestimated. Due to the large basis-state mixing of the ^2P_J states, the binding energies of peaks 15–18 were found to be the most sensitive to the configuration interaction and OL scheme. An approximately 200-meV shift to smaller binding energies was observed when the configuration space was ex-

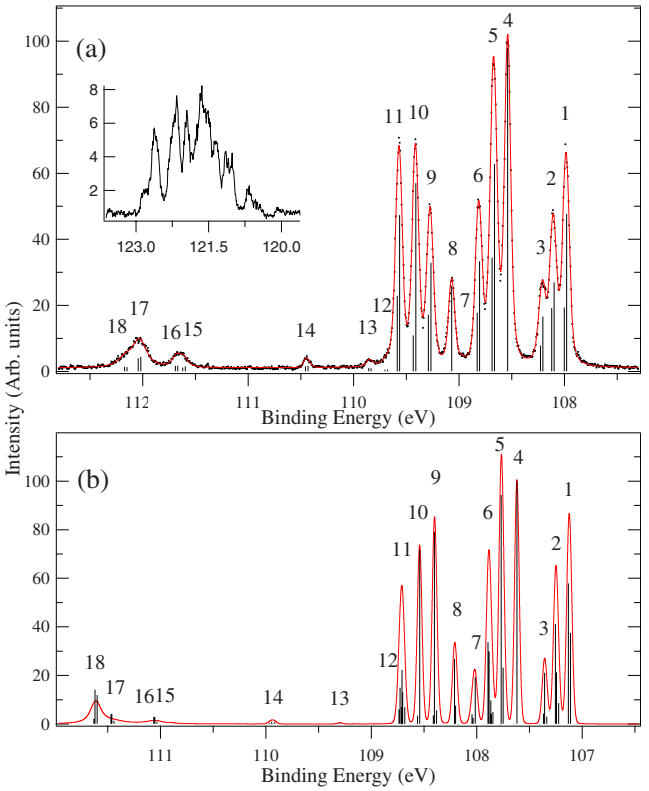

FIG. 1. (Color online) (a) Measured and (b) simulated $2p$ photoionization spectrum of atomic Si at the temperature of 1500 °C. The experimental data are shown as dots, and the solid (red) line is a fit to the data. Vertical bars in (a) indicate intensity from the fit. The spectrum in the upper left corner is the $2p$ satellite from $3p^2 \rightarrow 3p4p$ shakeup during photoionization. Vertical lines in (b) indicate calculated intensities from the initial states, and the red solid line is the convolved spectrum using experimental Gaussian and calculated Lorentzian linewidths.

panded from the single configuration to the final set. Change from the AL to the OL scheme decreased the splitting further, about 50 meV. Peaks 15–18 are also considerably wider than the other structures, due to faster Auger decay. The experimentally observed lifetime of states corresponding to peaks 1–11 is about 22 fs, whereas the lifetime of states $(^3P)\ ^2P_{1/2}$ and $(^1S)\ ^2P_{3/2}$ is about 4 fs. The calculated lifetime broadenings were underestimated, which appears as narrower lines in Fig. 1(b). Suppression of low-spin multiplets has also been observed in $3p$ ionization of $3d$ transition metals and explained by a fast Coster-Kronig transition [29]. The origin of the suppression in this case is essentially different, resulting from the exceptionally large angular integrals of the $2p^{-1}3s^23p^2 \rightarrow 2p^63s3p\ ^3P_{0,1,2}$ Auger amplitudes to the ϵs continuum. Similar behavior has been reported recently on the $2p^63s^23p \rightarrow 2p^{-1}3s^23p\ ^1S_0$ photoionization of atomic Al [15].

$2p$ ionization of the neighbor element Al displayed a fine competition between Coulomb and spin-orbit interactions [15]. In Si an additional electron in the $3p$ shell changes the situation drastically. The Coulomb interaction between the $3p$ electrons overruns the spin-orbit interaction of the $2p$ hole completely. The $2p$ ionic configuration is split by direct Coulomb interaction into P, D, and S groups, which are further separated to high-spin $(2S+1=4)$ and low-spin $(2S+1=2)$ components by the exchange interaction. This interaction causes a splitting of 4 eV between the ^4P and ^2P components (peaks 1–3 and 15–18, respectively, in Table II). The J dependence between the same L and S states, which results from spin-orbit interaction, produces a splitting of 0.2 eV inside the ^4P_J triplet (peaks 1–3). A comparison to Table I shows that the opening of the $2p$ shell causes an order of magnitude larger spin-orbit splitting for the $^4P_{5/2,3/2,1/2}$ triplet than for the $^3P_{0,1,2}$ triplet in the neutral initial configuration.

The main structures are further discussed next with the aid of Figs. 2(a)–2(e) depicting the individual calculated spectra from five initial states summed in Fig. 1(b). The initial-state splitting (Table I) is scaled off, and the binding energy axis is correct for the spectrum in Fig. 2(a). The left-hand axis of Fig. 2 shows the relative intensity of each initial state at the temperature of 1500 °C, and the right-hand axis shows the cross section in Mb. Figures 2(a)–2(e) show very large deviations in photoionization cross sections for different initial states. Interestingly, the sum of completely different photoelectron spectra from the three populated initial states [Figs. 2(a)–2(c)] forms a spectrum in Fig. 1 which is quite close to the $(2J_f+1)$ statistical distribution of $^4P_{J_f}$ $(J_f=5/2,3/2,1/2)$ and $^4D_{J_f}$ $(J_f=7/2,5/2,3/2,1/2)$ groups. This is because the thermal Boltzmann distribution at the current temperatures is very close to the degeneracy of the initial states. This cancels the initial-state degeneracy factor $(2J_i+1)$ in the denominator of the photoionization matrix elements [see, e.g., Eq. (3) from Ref. [15]], thus leaving only the dependence of the final-state degeneracy $(2J_f+1)$ and radial dipole-matrix elements.

Comparing Figs. 1(a) and 1(b) a fairly good agreement between calculated and experimental intensities is seen. Deviation in peaks 5 and 9 are due to an overestimation of the ϵd radial continuum-matrix elements from the $^3P_1$ initial state in our theoretical treatment. A distinct feature is an anomalous behavior of peak 7 assigned as a transition to the $(^1D)\ ^2P_{3/2}$ final state. The peak is due to transitions to one of the three states having the $^2P_{3/2}$ final LSJ term. The state is heavily mixed via exchange interaction with a purity of only 0.34 in the LSJ basis (0.64 in the jj basis). We consider that the energy of the state is correctly calculated. A shift of about 150 meV is required to overlap peak 7 with other structures. A maximum oscillation of only ± 10 meV was seen when moving from the single-configuration approximation to the final CSF set. Also, if the peak overlaps with other structures, modifications due to additional intensity would be seen in the experiment. Our preliminary experiments also show that transitions corresponding to this peak are, however, present in the electron-excited Auger spectra. All of our calculations predicted considerable dipole photoionization amplitudes from all initial states for this line. Comparison to the experiment in Fig. 1(a) indicates that some cancellation effect which is not fully accounted for in calculations takes place as the intensity of the peak is completely missing in experiment. A cancellation resulting from radial integrals can be most likely ruled out because according to our calculations the relative intensity of peak 7 does not seem to vary as a

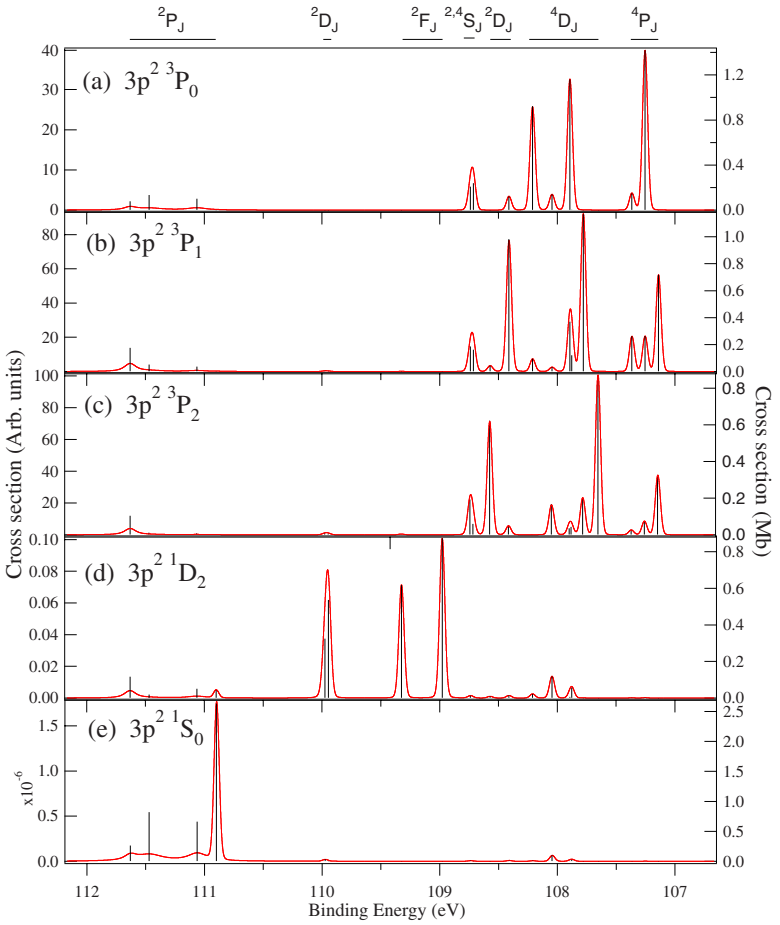

FIG. 2. (Color online) Calculated 2*p* photoionization cross sections of atomic Si from five initial states of the [Ne]$3s^3 3p^2$ configuration. Vertical lines indicate calculated intensities, and the red solid line is the convolved spectrum using experimental Gaussian and calculated Lorentzian linewidth. The left axis gives the relative intensity of different components at the temperature of 1500 °C, and the right axis displays the partial cross section in units of Mb at the photon energy of 140 eV.

function of photon energy. The occurrence of somewhat similar quasiforbidden transitions was discussed in Ref. [30] and also accounted for in our calculations as shown in the case of the 2*p* ionization of Al [15].

B. 2*p* Auger decay of atomic Si

Figures 3(a) and 3(b) show experimental and calculated overviews of the $2p^{-1}3s^2 3p^2 \rightarrow 2p^6 nln'l'$ Auger electron spectrum of atomic Si. The numbers in Fig. 3(a) refer to the populated Auger final states listed in Table III and horizontal lines correspond to the total 2*p* ionic-state fine-structure splitting. Group assignments were done by using information from calculations and experimentally determined splittings of Si^{2+} configurations from Ref. [27]. The group intensities in Table III are given as percentages from the total intensity. Auger transitions from $2p^{-1}3s^2 3p4p$ satellite and $2p^{-1}3s^2 3p$ doubly ionized initial states are labeled as "sat." The structures were identified experimentally by comparing the spectrum in Fig. 3(a) to a spectrum recorded using the photon energy below the satellite ionization threshold. A small structure from these satellite initial states seen at the kinetic energy of 97.5 eV is not shown in Fig. 3(a).

In order to ease the comparison between the experiment and calculated Auger spectra, experimentally obtained populations of Si^+ intermediate states from Table II were used in generating the simulated Auger spectrum in Fig. 3(b). In the cases of unresolved lines forming peaks 6, 11, and 14 (Table II), calculated intensity ratios were used. The same Lorentzian width was used for all lines in Fig. 3(b), which causes peaks at the kinetic energy of 82 eV and 88 eV to appear narrower than in the experiment.

The simulated spectrum in Fig. 3(b) shows that the total energy of Si^{2+} is well predicted, as well as experimental and calculated center-of-gravity energy splittings of the different final states. As shown in Table III, good *LS*-coupling conditions are restored in the Si^{2+} valence ionic configurations populated by Auger decay. Only the states $3p^2\ ^1D_2$ and $3s3d\ ^1D_2$ are considerably mixed. In contrast to the energy ordering of the neutral atomic states (see Table I) and what is expected from Hund's rules, $3p^2$-$3s3d$ mixing shifts the $3p^2\ ^1D_2$ singlet to appear at about 1 eV lower binding energy than the $3p^2\ ^3P$ triplet. An about 1.7 times larger spin-orbit splitting of the $3s^0 3p^2\ ^3P_{0,1,2}$ states of Si^{2+} [27] compared to the ground-state configuration states $3s^2 3p^2\ ^3P_{0,1,2}$ is expected because of the larger Coulomb potential field felt by the 3*p* electrons.

In the 2*p* Auger decay of Al, electron correlation in the 2*p* ionized states was found to cause drastic changes to the Auger decay patterns [15]. Similar effects are seen in Si. The $2p^6 3s^2$ and $2p^6 3s3p$ Auger final states are mainly populated directly from the $2p^{-1}3s^2 3p^2$ configuration. But, for example, Auger transitions to 3*p*3*d* final-state configuration [regions 9 and 10 in Fig. 3(a)] and some more subtle changes are due to configuration mixing in the 2*p* single-ionized state.

Considering the complexity of the experimental 2*p* Auger spectrum in Fig. 3(a), the overall agreement between experi-

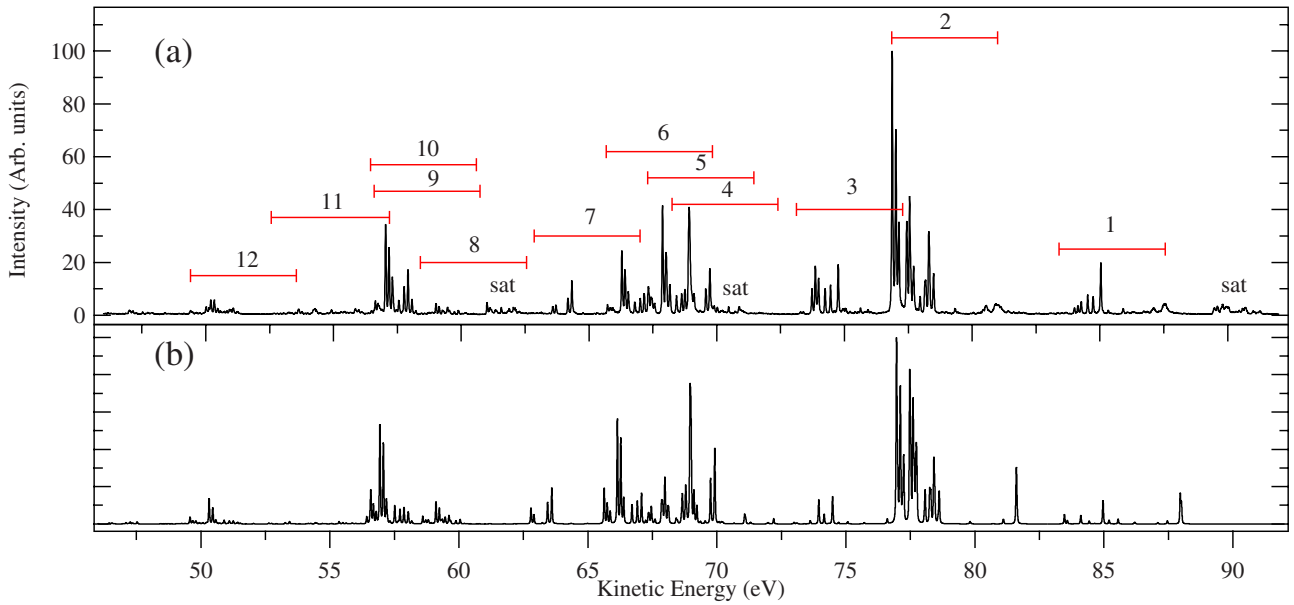

FIG. 3. (Color online) Experimental (a) and calculated (b) $2p$ Auger electron spectrum of atomic Si at a temperature of 1500 °C. Numbers refer to different final states given in Table III, and the horizontal lines correspond to total fine-structure splitting of $2p$-ionized states.

ment and simulated spectrum in Fig. 3(b) is good. The total intensity distributed between final states is well in line with the experiment. All major structures observed in the experiment are seen in the simulated spectrum without any additional groups predicted. Table III shows only the final states which are populated considerably. The region covers also many different Si^{2+} final states which are not populated via Auger decay, even though the transitions are in principle allowed by the selection rules. For example, between final states numbered 6 and 7 in Fig. 3(a) there are even-parity states $3s4s\ ^3S_1$, $3p^2\ ^1S_0$, and $3s4s\ ^1S_0$, which were found to receive only a negligible intensity. The intensity distributed to the $3s4s\ ^3S_1$ and $3s4s\ ^1S_0$ states is small because the mixing of the $2p^{-1}3s^23p^2$ configuration with other configurations where one or two electrons from the valence shells are excited to $4s$ orbital is negligible. The final state $3s^2\ ^1S_0$ (group number 1) is the only one with $L=0$ populated by the $2p$ Auger decay. The total intensity of the group is still much smaller than what can be expected intuitively. One reason is the parity of the final state, because conservation of parity prohibits the ϵs-electron emission in the $2p^{-1}3s^23p^2 \rightarrow 2p^63s^2+\epsilon l$ Auger decay. Matrix elements with ϵs continuum symmetry allowed are in general at least about one order of magnitude larger than matrix elements with higher (orbital) angular momentum.

TABLE III. Experimental and calculated intensity weighted center-of-gravity kinetic energies and total intensities of resolved Auger decay $[\mathrm{Ne}]nl^1n'l'^1$ final states. Column $|c_1^{LS}|^2$ gives the purities of the leading configurations in LSJ coupling. For triplets an average purity of the three lines is given.

		Experiment		Theory		
	Assignment	E_k (eV)	Int.	E_k (eV)	Int.	$\lvert c_1^{LS}\rvert^2$
1	$3s^2\ ^1S_0$	85.7	6.8	86.1	3.7	0.95
2	$3s3p\ ^3P_{0,1,2}$	77.7	36.2	77.8	38.6	1.00
3	$3s3p\ ^2P_1$	74.8	8.2	75.2	3.4	0.96
4	$3p^2\ ^1D_2$	69.3	2.6	69.8	5.9	0.64
5	$3p^2\ ^3P_{0,1,2}$	68.3	17.2	68.5	15.8	1.00
6	$3s3d\ ^3D_{1,2,3}$	66.8	7.9	66.3	11.6	1.00
7	$3s3d\ ^1D_2$	64.0	3.6	63.4	2.8	0.64
8	$3s4d\ ^3D$, $3p3d\ ^3F$	59.3	1.7	59.2	3.0	
9	$3p3d^3P_{0,1,2}$	57.1	2.0	56.9	3.0	0.92
10	$3p3d\ ^3D_{1,2,3}$	57.3	8.9	57.2	8.6	0.77
11	$3p4p\ ^3P, ^1D_2$	54.3	1.7	54.5	0.7	
12	$3p4d\ ^3D, ^3P$	50.4	3.1	50.4	2.7	

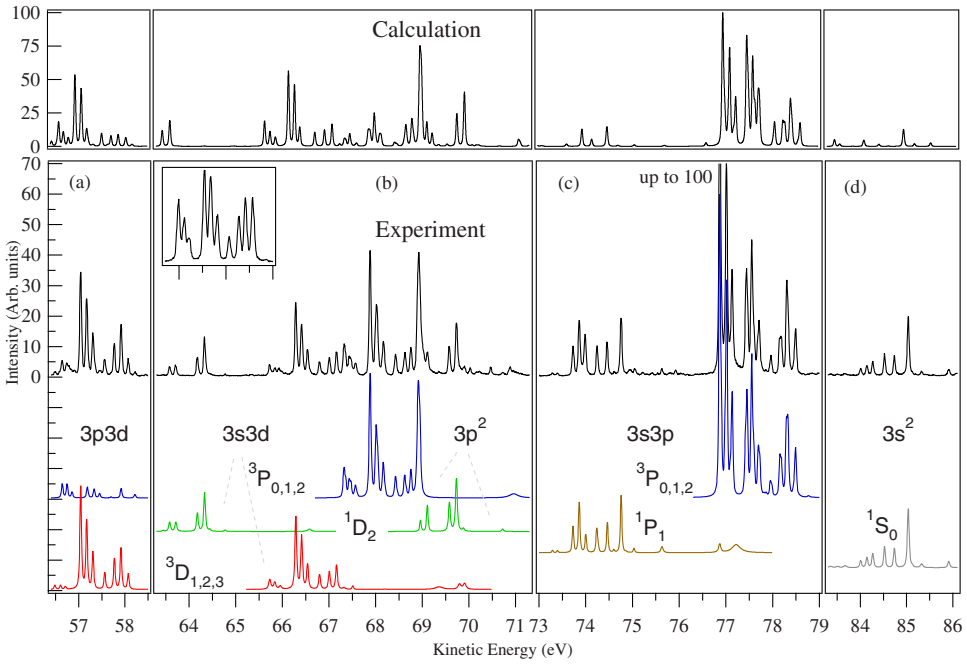

FIG. 4. (Color online) Calculated (upper panels) and experimental (lower panels) magnified regions of the 2*p* Auger spectrum of Si. Solid colored curves below the experimental spectrum show fitting results to different final states. Same height and color indicate the same *LSJ* term given in the figure. Panel (a) shows two final states from the [Ne]3*p*3*d* configuration, panel (b) two final states from [Ne]3*s*3*d* and [Ne]$3p^2$ configurations, panel (c) two final states from the [Ne]3*s*3*p* configuration, and panel (d) the singlet state from the [Ne]$3s^2$ configuration. The upper left corner of panel (b) shows the main lines of the 2*p* photoelectron spectrum on the same energy scale.

Mg-like Si with two electrons above the closed-shell structure of neon is perhaps the simplest nontrivial case to study how the Auger decay pathways depend on the configurations with the same coupled *LSJ* term and how the pattern depends on the different *LSJ* terms coupled from the same configuration. Figure 4 shows magnified experimental fitting results to nine selected final states together with calculations, and Table IV lists individual line intensities to these final states.

1. Singlet final states

Figure 4 shows that none of the Auger decay patterns to different final states resemble the initial-state distribution shown in the upper left corner of panel (b) [or Fig. 1(a)]. Especially, Auger decay patterns to singlet final states show very characteristic behavior. Despite the different L and J quantum numbers and parity, transitions to the $3s^2\ ^1S_0$ and $3s3p\ ^1P_1$ states are quite similar (see Table IV). The Auger transitions from 2*p*-ionized fine-structure states ^4P_J and $^2D_{5/2}$ are clearly unfavored in both cases. The patterns deviate strongly only on transitions from ^4D_J (J=7/2,5/2,3/2) initial states. Table IV and Fig. 4, panels (c) and (d), show that the correspondence between the experiment and calculation in the case of individual lines related to the final states $3s^2\ ^1S_0$ and $3s3p\ ^1P_1$ is not so good. In our MCDF calculations there seem to be instabilities related to the CSF expansions of some final states, where several quite large Auger amplitudes with opposite signs from different CSFs cancel each other. This cancellation is very sensitive to the mixing coefficients and Auger matrix elements. A deviation of a few percent in the matrix elements can cause drastic changes to the results. A good agreement is found for Auger transitions to the $3p^2\ ^1S_0$ final states where nearly complete cancellation of matrix elements causes the missing intensity.

Interestingly the $3p^2\ ^1D_2$ and $3s3d\ ^1D_2$ final states are mainly reached from the $^4D_{5/2,3/2}$ and $^2D_{5/2,3/2}$ initial states (Table IV). The Auger emission patterns to these final states are nearly identical because of a considerable $3p^2-3s3d$ mixing between the final states. In summation of Auger rates [Eq. (2)] to the $3s3d\ ^1D_2$ and $3p^2\ ^1D_2$ states, the largest rates arise from transitions from identical initial-state CSFs to identical final-state CSFs. In these cases the Auger initial-state CSFs are coupled from the $2p^{-1}3p^4$ configuration and the final states from the $2p^63p^2$ configuration. Also, because the initial-state CSFs come from the $2p^{-1}3p^4$ configuration, the Auger transitions to these final states arise entirely from configuration mixing.

2. Triplet final states

The richer structures seen in the triplet final states as compared to the singlet states are easily understood because in triplets each peak is a sum of three lines with different total J quantum number not resolved in the experiment. Many overlapping transitions obviously tend to smear out the most distinct spectral features. The population of the $^3P_{0,1,2}$ triplet states in panels (a), (b), and (c) of Fig. 4 shows quite large differences. The $2p^{-1}3s^23p^2\ ^4P_{5/2,3/2,1/2}$ states prefer to decay to the $3s3p\ ^3P_{0,1,2}$ states, which is explained by the large matrix elements for ϵs continuum waves. Further, the same continuum symmetry may cause the observed overall similarities in the transitions to $^3P_{0,1,2}$ triplets of 3*s*3*p* and 3*p*3*d* configurations.

The decay pattern to $3p^2\ ^3P_{0,1,2}$ final states in Fig. 4(b) is well predicted with the exception of the underestimated transition strength from the $2p^{-1}3s^23p^2\ ^4D_{5/2,3/2,1/2}$ initial states (Table IV). In Auger transitions to the $3p^2\ ^3P_{0,1,2}$ final states the largest contributing matrix elements have initial-state CSFs coupled from the $2p^{-1}3p^4$ configuration. The matrix elements with CSFs coupled from the $2p^{-1}3p^4$ configuration mixing with the $2p^{-1}3s^23p^2\ ^4D_{5/2,3/2,1/2}$ states cancel completely, and the (underestimated) intensity seen in the calcu-

TABLE IV. Experimental and calculated Auger intensities from individual initial states to nine selected final states. Intensities are given as percentages from the total population of the final state.

	Experiment								
	Final state								
Initial	$3s^2$	$3s3p$		$3p^2$		$3s3d$		$3p3d$	
state	^1S	^3P	^1P	^1D	^3P	^3D	^1D	^3D	^3P
$^4P_{5/2}$	1.1	21.9	0.0	0.0	6.8	4.7	1.1	1.1	19.5
$^4P_{3/2}$	1.0	15.7	0.7	0.0	4.7	3.3	0.8	1.1	19.1
$^4P_{1/2}$	1.6	7.7	0.6	0.8	2.4	1.6	1.6	0.7	8.0
$^4D_{7/2}$	3.1	9.6	8.9	0.0	22.0	26.7	1.0	31.8	15.3
$^4D_{5/2}$	4.4	11.9	17.1	7.5	6.5	19.3	10.4	20.9	12.6
$^2P_{1/2}$, $^4D_{3/2}$	6.0	4.9	6.5	17.7	6.5	8.3	11.3	11.3	6.1
$^4D_{1/2}$	8.3	1.5	9.6	0.0	4.0	5.5	0.0	4.9	1.3
$^2D_{3/2}$	7.8	4.4	10.1	24.3	4.2	6.6	19.4	9.3	13.4
$^2D_{5/2}$	0.0	8.8	0.8	44.6	4.5	9.1	39.8	12.6	0.0
$^2S_{1/2}$, $^4S_{3/2}$	26.1	3.9	19.1	3.1	32.0	5.2	1.7	4.6	4.8
$^2F_{7/2}$	0.3	0.1	0.2	2.0	0.0	0.0	0.0	0.0	0.0
$^2F_{5/2}$	2.1	0.2	1.3	0.0	0.0	1.1	1.4	0.0	0.0
$^2D_{5/2}$, $^2D_{3/2}$	3.1	0.8	3.3	0.0	0.0	0.2	1.4	0.1	0.0
$\Sigma_J {}^2P_J$	35.0	8.7	22.4	0.0	6.4	12.9	10.3	1.8	0.0
	Calculation								
$^4P_{5/2}$	0.0	18.3	0.0	0.4	3.2	9.7	0.4	2.7	36.2
$^4P_{3/2}$	8.4	12.2	1.6	0.0	3.7	5.6	0.1	1.3	21.1
$^4P_{1/2}$	3.0	6.8	0.3	0.0	1.1	3.2	0.1	0.7	12.5
$^4D_{7/2}$	0.3	14.9	0.1	0.0	7.9	28.8	0.1	37.0	7.5
$^4D_{5/2}$	0.0	13.7	0.0	17.2	10.5	23.4	18.1	28.5	7.3
$^2P_{1/2}$, $^4D_{3/2}$	8.0	9.2	3.3	9.7	5.5	7.1	10.6	8.1	2.9
$^4D_{1/2}$	2.6	3.2	22.4	1.0	1.5	5.4	1.0	6.8	2.4
$^2D_{3/2}$	0.5	5.2	9.3	24.5	7.5	6.3	24.7	5.5	2.8
$^2D_{5/2}$	0.0	7.2	0.2	41.0	9.4	8.5	40.8	5.6	3.2
$^2S_{1/2}$, $^4S_{3/2}$	21.4	3.1	26.7	1.0	45.3	0.9	0.5	3.8	3.4
$^2F_{7/2}$	3.3	0.0	1.4	0.1	0.0	0.1	0.1	0.0	0.0
$^2F_{5/2}$	4.3	0.0	2.1	0.4	0.2	0.2	0.4	0.0	0.0
$^2D_{5/2}$, $^2D_{3/2}$	1.9	0.2	1.4	1.1	0.8	0.1	0.7	0.0	0.0
$\Sigma_J {}^2P_J$	46.3	5.9	30.9	3.6	3.3	0.7	2.6	0.0	0.6

lation comes from the matrix elements with initial-state CSFs from the $2p^{-1}3s^23p^2$ configuration.

Auger decay patterns to the $3p3d\ ^3D_{1,2,3}$ and $3s3d\ ^3D_{1,2,3}$ states are nearly identical, even though the parity of the final states is opposite. Besides the fact that the final-state *LSJ* term is the same, a common factor in these transitions is the initial state. The largest Auger amplitudes to these states come from exactly the same CSFs coupled from the $2p^{-1}3s3p^23d$ initial-state configuration. This shows that at least in Si under good *LS*-coupling conditions, the same initial-state CSFs and the same final-state *LSJ* term produce nearly identical Auger decay patterns.

V. CONCLUSIONS

$2p$ ionization and Auger decay of atomic silicon were studied experimentally and theoretically. The binding energy and fine-structure splittings of Si $2p$-ionized states were determined with high precision. Good overall agreement was obtained between theoretical and calculated $2p$ photoionization cross sections. All major structures in the experimental $2p$ Auger electron spectrum were assigned, and very good agreement between the experiment and theoretical prediction was seen. The intensity distribution to different Auger final states was discussed in detail with the aid of state-of-the-art Auger decay calculations. In the experimental photoelectron spectrum, an unpredicted cancellation effect was seen and more theoretical work, left for future studies, is needed.

ACKNOWLEDGMENTS

This work has been financially supported by the Research Council for Natural Sciences of the Academy of Finland and

the European Community-Research Infrastructure Action under the FP6 "Structuring the European Research Area" Program (through the Integrated Infrastructure Initiative "Integrating Activity on Synchrotron and Free Electron Laser Science"). K.J. would like to thank support from the Vilho, Yrjö and Kalle Väisälä foundation. S.U. was financed by the Marie Curie Early Stage Training Site MAXLAS (Grant No. MEST-CT-2005-020356) within the 6th European Community Framework Programme. S.F. acknowledges support by the DFG under Project No. FR 1251/13. We thank also the staff of MAX-laboratory for their assistance during the experiments.

[1] K. Fuke, K. Tsukamoto, and F. Misaizu, Z. Phys. D **26**, 204 (1993).
[2] C. F. Hirjibehedin, C.-Y. Lin, A. F. Otte, M. Ternes, C. P. Lutz, B. A. Jones, and A. J. Heinrich, Science **317**, 1199 (2007).
[3] J. D. Bozek, G. M. Bancroft, and K. H. Tan, Phys. Rev. A **43**, 3597 (1991).
[4] T. D. Thomas, C. Miron, K. Wiesner, P. Morin, T. X. Carroll, and L. J. Saethre, Phys. Rev. Lett. **89**, 223001 (2002).
[5] A. Gheorghiu, C. Sénémaud, H. Roulet, G. Dufour, T. Moreno, S. Bodeur, C. Reynaud, M. Cauchetier, and M. Luce, J. Appl. Phys. **71**, 4118 (1992).
[6] B. H. Boo, S. M. Park, and I. Koyano, J. Phys. Chem. **99**, 13362 (1995).
[7] R. E. Honig, RCA Rev. **23**, 567 (1962); R. E. Honig and D. A. Kramer, *ibid.* **30**, 285 (1969).
[8] J. T. Costello, E. T. Kennedy, J.-P. Mosnier, M. H. Sayyad, and C. McGuinness, J. Phys. B **31**, L547 (1998).
[9] H. van Brug, K. Murakami, F. Bijkerk, and M. J. van der Wiel, J. Appl. Phys. **60**, 3438 (1986).
[10] T. Ohyanagi, A. Miashita, K. Murakami, and O. Yoda, Jpn. J. Appl. Phys., Part 1 **33**, 2586 (1994).
[11] J.-P. Mosnier, M. H. Sayyad, E. T. Kennedy, J.-M. Bizau, D. Cubaynes, F. J. Wuilleumier, J.-P. Champeaux, C. Blancard, R. H. Varma, T. Banerjee, P. C. Deshmukh, and S. T. Manson, Phys. Rev. A **68**, 052712 (2003).
[12] D. A. Verner, G. J. Ferland, K. T. Korista, and D. G. Yakolev, Astrophys. J. **465**, 487 (1996).
[13] M. Huttula, S. Heinäsmäki, H. Aksela, E. Kukk, and S. Aksela, J. Electron Spectrosc. Relat. Phenom. **156-158**, 270 (2007).
[14] M. Huttula, K. Jänkälä, A. Mäkinen, H. Aksela, and S. Aksela, New J. Phys. **10**, 013009 (2008).
[15] K. Jänkälä, S. Fritzsche, M. Huttula, J. Schulz, S. Urpelainen, S. Heinäsmäki, S. Aksela, and H. Aksela, J. Phys. B **40**, 3435 (2007).
[16] K. Jänkälä, J. Schulz, M. Huttula, A. Caló, S. Urpelainen, S. Heinäsmäki, S. Fritzsche, S. Svensson, S. Aksela, and H. Aksela, Phys. Rev. A **74**, 062704 (2006).
[17] C. G. King, M. Tronc, F. H. Read, and R. C. Bradford, J. Phys. B **10**, 2479 (1977).
[18] J. Jauhiainen, A. Ausmees, A. Kivimäki, S. J. Osborne, A. Naves de Briton, S. Aksela, S. Svensson, and H. Aksela, J. Electron Spectrosc. Relat. Phenom. **69**, 181 (1994).
[19] F. A. Parpia, C. Froese Fischer, and I. P. Grant, Comput. Phys. Commun. **94**, 249 (1996).
[20] S. Fritzsche, C. Froese Fischer, and G. Gaigalas, Comput. Phys. Commun. **148**, 103 (2002).
[21] G. Gaigalas, T. Zalandauskas, and S. Fritzsche, Comput. Phys. Commun. **157**, 239 (2004).
[22] S. Fritzsche, J. Electron Spectrosc. Relat. Phenom. **114-116**, 1155 (2001).
[23] S. Fritzsche, A. Surzhykov, and T. Stöhlker, Phys. Rev. A **72**, 012704 (2005).
[24] S. Fritzsche, J. Nikkinen, S.-M. Huttula, H. Aksela, M. Huttula, and S. Aksela, Phys. Rev. A **75**, 012501 (2007).
[25] K. Jänkälä, R. Sankari, J. Schulz, M. Huttula, A. Calo, S. Heinäsmäki, S. Fritzsche, T. Rander, S. Svensson, S. Aksela, and H. Aksela, Phys. Rev. A **73**, 022720 (2006).
[26] R. D. Cowan, *The Theory of Atomic Structure and Spectra* (University of California Press, Berkeley, 1981).
[27] http://physics.nist.gov/PhysRefData/ASD/
[28] K. Jänkälä, J. Schulz, and H. Aksela, J. Electron Spectrosc. Relat. Phenom. **161**, 95 (2007).
[29] A. von dem Borne, R. L. Johnson, B. Sonntag, M. Talkenberg, A. Verweyen, Ph. Wernet, J. Schulz, K. Tiedtke, Ch. Gerth, B. Obst, P. Zimmermann, and J. E. Hansen, Phys. Rev. A **62**, 052703 (2000).
[30] D. Cubaynes, M. Meyer, A. N. Grum-Grzhimailo, J.-M. Bizau, E. T. Kennedy, J. Bozek, M. Martins, S. Canton, B. Rude, N. Berrah, and F. J. Wuilleumier, Phys. Rev. Lett. **92**, 233002 (2004).